

# Fast Molecular Compression by a Hyperthermal Collision Gives Bond-Selective Mechanochemistry

Lukas Krumbein<sup>†,1</sup>, Kelvin Anggara<sup>†,1</sup>, Martina Stella<sup>2</sup>, Tomasz Michnowicz<sup>1</sup>, Hannah Ochner<sup>1</sup>, Sabine Abb<sup>1</sup>, Gordon Rinke<sup>1</sup>, André Portz<sup>3</sup>, Michael Dürr<sup>3</sup>, Uta Schlickum<sup>1,4</sup>, Andrew Baldwin<sup>5</sup>, Andrea Floris<sup>6</sup>, Klaus Kern<sup>1,7</sup>, Stephan Rauschenbach<sup>1,5\*</sup>

<sup>1</sup>*Max-Planck-Institut für Festkörperforschung, Heisenbergstrasse 1, DE-70569 Stuttgart, Germany.*

<sup>2</sup>*Department of Materials, Royal School of Mines, Imperial College London, Exhibition Road, London, SW7 2A2, United Kingdom.*

<sup>3</sup>*Institut für Angewandte Physik, Justus-Liebig-Universität Giessen, Heinrich-Buff-Ring 16, DE-35392 Giessen, Germany.*

<sup>4</sup>*Institut für Angewandte Physik, Technische Universität Braunschweig, Mendelssohnstrasse 2, DE-38106 Braunschweig, Germany.*

<sup>5</sup>*Chemistry Research Laboratory, Department of Chemistry, University of Oxford, 12 Mansfield Road, Oxford, OX1 3TA, United Kingdom.*

<sup>6</sup>*School of Chemistry, University of Lincoln, Brayford Pool, LN6 7TS, Lincoln, United Kingdom.*

<sup>7</sup>*Institut de Physique, École Polytechnique Fédérale de Lausanne, Laussane, CH-1015, Switzerland.*

\*Corresponding Author: [stephan.rauschenbach@chem.ox.ac.uk](mailto:stephan.rauschenbach@chem.ox.ac.uk)

<sup>†</sup>equal contributions

## **CLASSIFICATION:**

Physical Sciences – Physics

## **KEYWORDS**

Bond-selective reaction, Gas-surface dynamics, Mechanochemistry

**ABSTRACT**

**Elucidating mechanisms of a selective chemical reaction is fundamental towards control over its outcome. For molecules colliding on a surface, accelerating the molecule towards the surface has not been considered as a means to attain a selective reaction. Here we show bond-selective reaction of a molecule induced by its translational kinetic energy towards a surface. We use electrospray ion beam deposition to collide the molecule at low, hyperthermal translational energy (2 - 50 eV) with a Cu(100) surface and image the outcome at single-molecule level using Scanning Tunneling Microscopy (STM). A large mechanical impulse generated from the collision compresses the molecule and bends specific bonds within, making them react selectively. The compression-induced dynamics leads to reaction products that are inaccessible by thermal pathways since the compression timescale (~sub-picoseconds) is much shorter than the thermalization timescale (~nanoseconds or longer). The bond-selective, compression-induced chemistry, exemplified here by an organic dye molecule (Reichardt's Dye,  $C_{41}H_{30}NO^+$ ) colliding on a Cu-surface allows the exploration of mechanochemistry, especially for large molecules possessing complex chemical functionality that may have limited thermal stability.**

## **SIGNIFICANCE**

*In colliding molecules with a surface, we discovered a novel chemically selective reaction mechanism. The selectivity emerges from large, nanonewton force compressing the molecule within subpicoseconds upon its crash on surface. The fast and systemic compression drives the system to seek reactive pathways that are thermally inaccessible, thereby yielding reaction products that are unobtainable thermally. The experiment is based on technologies generally available in modern chemistry laboratories: electrospray ionization mass spectrometry modified for deposition offers control of the collision energy. Compression-induced reactions reported here offer the use of mechanochemistry to graft large, thermally sensitive molecules at surfaces and to explore molecular reactions and conformations inaccessible by thermal means – the latter being key to structural investigations of biomolecules.*

## **MAIN TEXT**

Chemistry is concerned with the manipulation of bonds between atoms with the goal to use chemical reactions to form desired substances. Achieving this goal requires an understanding of how selectivity emerges. Chemical reactions that occur following a molecule-surface collisions are important, technologically and for fundamental studies, in fields as diverse as heterogeneous catalysis (1–9), epitaxial material fabrication (10–12), biomolecular analysis (13–17), and astrochemistry (10). Bond-selective reactions in a molecule-surface collision have been demonstrated by exciting specific vibrational modes of a molecule right before its surface impact (5, 7, 8). This approach succeeds due to the sudden energy accumulation in a specific molecular degree-of-freedom triggering a reaction that promptly occurs before the deposited energy spreads to other degrees-of-freedom not involved in the reaction, i.e. before thermalization (18, 19).

Imparting energy into the molecular center-of-mass motion (i.e. translation) towards the surface offers an alternative means to induce surface reactions, which is attractive because translational energy of a molecular ion is readily achieved by acceleration in an electric field. However, simply accelerating molecules towards the surface has been deemed unsuitable for obtaining bond-selective reactions, because the collision excites soft modes of the molecule (20, 21) which are poorly coupled to stiff stretching modes that promote bond-breaking reactions (9, 19). As a result, reactions would happen late after the thermalization occurs which diverges reaction pathways towards non-selective outcomes (10, 22–26).

It remains unclear whether excited soft modes in the absence of thermalization could give a selective reaction because previous studies have only detected the reaction products in the gas-phase (10, 22–26) whereby excess energy from the collision cannot be removed from the molecular product and subsequently cause further reactions. We avoid this issue by using the

surface to remove excess energy from the collision products. This is readily achieved by carrying out the experiment at lower, near-threshold energies, which necessitates the detection of the adsorbed collision outcome *on surface*.

Here we show that the large excitation of soft modes in a molecule surface collision, i.e. extensive compression of a molecule, occurring at timescales faster than thermalization, does lead to a selective, non-thermal reaction path. We have used scanning tunneling microscopy (STM) to detect the surface-bound products from collisions between a large molecular ions and a metal surface, carried out at low hyperthermal energies (2 – 50 eV). Singly-protonated Reichardt's Dye (**RD**,  $\text{C}_{41}\text{H}_{30}\text{NO}^+$ ) was collided at normal incident angle with a Cu(100) surface held at room temperature using electrospray ion beam deposition (ES-IBD) (27). The collision outcome, examined by STM at 11 K (see Supplementary Fig 1), revealed reactive pathways that selectively cleaved a single C-N bond in RD. Energy-dependent experiments and *ab-initio* Molecular Dynamics (MD) calculations revealed orientation-dependent dynamics that selectively bend specific C-N bonds in the molecule, ignoring the minimum energy path.

Our work gives insight into the emergence of bond-selective mechanochemical reactions in molecule-surface collisions. Collision-induced mechanochemistry (28, 29) promises to be generally applicable to large molecules such as peptides or even proteins (13–17), providing a new tool to perform non-thermal on-surface synthesis of novel molecular materials.

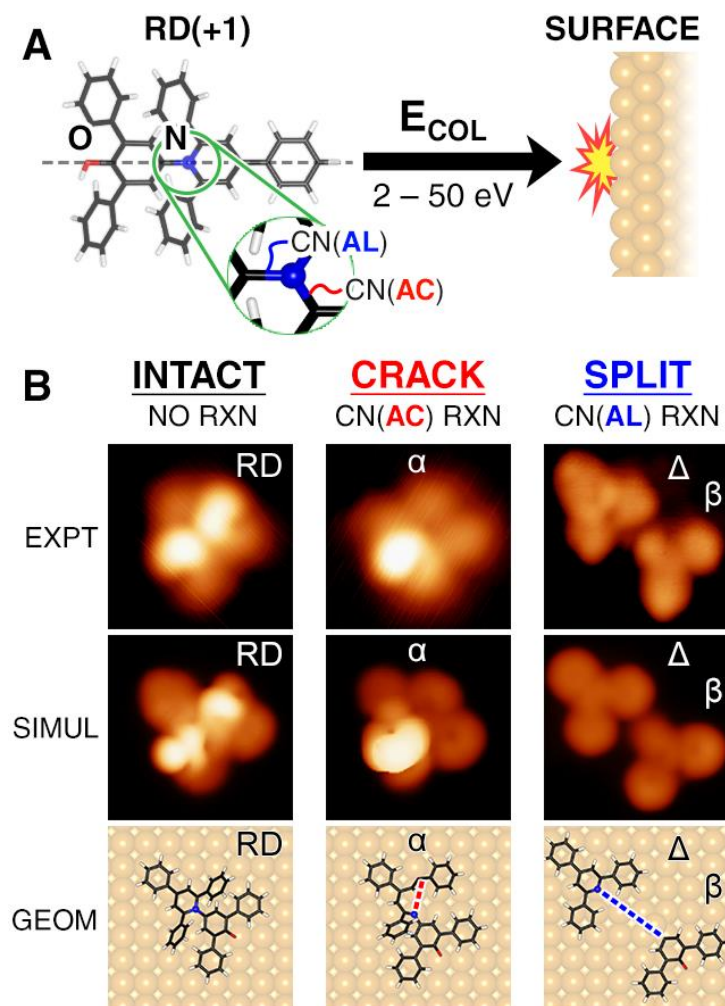


**Fig. 1. | Hyperthermal collision of Reichardt's Dye (RD) on Cu(100) surface.** **A.** Schematics of the experiment, showing a beam of singly-protonated RD(+1) aimed along the surface normal to the Cu-surface held at room temperature. Two types of C-N bond (see inset) are labeled as C-N(AC), and C-N(AL) based on their orientation against the N-O axis in RD (grey dashed line). **B.** STM image (EXPT) and simulation (SIMUL) of the three collision outcomes imaged at 11 K. The INTACT pathway gives an adsorbed RD. The CRACK pathway breaks a CN(AC) in the parent RD to give one  $\alpha$ -fragment, while the SPLIT pathway breaks the CN(AL) to give one  $\beta$ - and one  $\Delta$ -fragment. Computed geometries (GEOM) show a broken CN(AC) (red dashed line) in the  $\alpha$ -fragment, and a broken CN(AL) (blue dashed line) between  $\beta$ - and  $\Delta$ -fragment.

## EXPERIMENT

Figure 1 shows three outcomes obtained from the collision between an RD ion and a Cu(100) surface: one non-reactive, and two reactive outcomes, as revealed by STM imaging and simulation. These are the outcomes of specific collision dynamics that are accessed by aiming the ion beam at normal incidence angle to the surface, as shown in Fig 1A. The non-reactive pathway, INTACT, was found to yield an adsorbed intact RD with its two phenyl rings oriented vertical from the surface as shown in Fig 1B. We expect the proton that was attached to the O-atom in the RD ion to undergo spontaneous dehydrogenation on surface at room temperature given the low computed barrier of 0.08 eV.

The reactive pathways were found to be bond-selective to the C-N bonds, breaking either one out of the two types of C-N bonds in RD (see Fig 1A): the C-N bond pointing at an angle ‘across’ the N-O axis of the molecule, termed C-N(AC); or the C-N bond pointing ‘along’ the N-O axis, termed C-N(AL). In the CRACK pathway, a single C-N(AC) was broken to give a dissociated RD fragment ( $\alpha$ -fragment) as shown in Fig 1B. In the SPLIT pathway, the C-N(AL) bond was broken to give two products as shown in Fig 1B: a diphenylphenoxy ( $\beta$ -fragment), and a triphenylpyridine ( $\Delta$ -fragment). The observation of CRACK and SPLIT pathways thus establishes the existence of bond-selective pathways due to molecule-surface collision at hyperthermal translational energy.

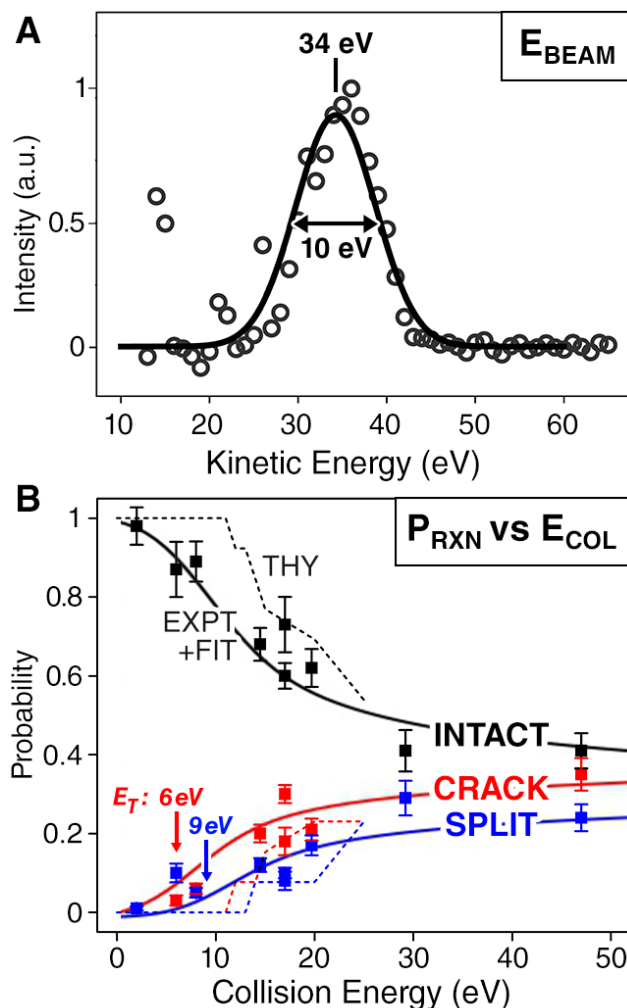


**Fig. 2. | Evidence of reactive collision by incident translational energy.** **A.** A typical energy profile of the RD ion beam. Gaussian fit (solid line) onto the data gives a peak of 34 eV, and an FWHM of 10 eV respectively. **B.** Probabilities to observe INTACT (black), CRACK (red), and SPLIT (blue) outcomes measured against the collision energies. The data points (solid square) were fitted with a reaction probability model (solid line) to give a threshold translational energy ( $E_T$ ) for each pathways (see Methods for details). The dashed line gives probability obtained from *ab-initio* molecular dynamics calculations. The error bar in each data points gives the standard deviation.

To gain insight into the dynamics of these bond-selective pathways, we measured their respective reaction probabilities against the kinetic energy of the molecular beam. We varied the collision energy by decelerating the ions approaching the surface, which shifted the energy



distribution of the ion beam (see Fig 2A) without changing its width (see Methods). Since the ion beam is aimed normal to the surface, the collision energy is the kinetic energy, which corresponds to the molecular translation along the surface normal. The result of this energy-dependent measurement was fitted to a model, inspired by the Sudden Vector Projection (SVP) description of molecular collisions at the gas-surface interface (19). We compute the reaction probability ( $P_{\text{RXN},X}$ ) for each pathway (X) by projecting the molecular translation vector to the reaction coordinate vector to estimate how much of the translation energy ( $E_{\text{COL}}$ ) is utilized to propel the system towards the transition state (see Supplementary Fig 2 and Methods for details). The model yields the relation:

$$P_X(E_{\text{COL}}) = P_{\text{SAT},X} \cos^{-1} \sqrt{\frac{E_{\text{T},X}}{E_{\text{COL}}}} \quad (1)$$

The fitting gave a translational energy threshold ( $E_{\text{T}}$  in Eq. (1)) of 6.0 eV for CRACK, and 9.5 eV for SPLIT, as shown in Fig 2B. The existence of this threshold, which marks the minimal energy needed for the reaction, thereby evidences the translational energy as the cause of the reaction, ruling out surface-to-molecule charge transfer(10, 24, 25) as a sole cause of the reaction.

Further dynamical insight is obtained by the observation of the reaction probabilities approaching a limiting value,  $P_{\text{SAT},X}$ , estimated to be 0.43 for CRACK, and 0.35 for SPLIT at high energies using Eq. 1. Such a saturation of reaction probability below unity has been observed in gas-surface scattering experiment (25, 30, 31), and in surface-induced dissociation of proteins (16). From the diatomic-surface scattering studies (30, 31), the saturation was understood to be due to a steric effect in which there was a limited range of orientations in the approaching molecule (also known as ‘cone of acceptance’ – see ref (32)) that upon collision

with the surface would lead to a reactive outcome. Such a strong dependence on initial orientation is characteristic of a *direct* reaction in which a *single-collision* event causes a *direct* energy transfer from the molecule translation into the reaction coordinate (1, 30, 31, 33). Transferring insights from the diatomic-surface scattering studies to the present work, the saturation in reaction probability observed for CRACK and SPLIT is therefore indicative of an orientation-dependent *direct* reactions caused by a *single-collision* event, ruling out a multi-collision event (33, 34) via a precursor state (35).

## THEORY

We corroborate this experimental inference by simulating the RD/Cu(100) collision by MD calculations, which revealed that CRACK and SPLIT are orientation-dependent *direct* reaction caused by a *single-collision* event (see Fig 3A and 4, Supplementary Movie 1 and 2). The collision was modeled as a positively-charged RD ion approaching a negatively-charged surface that was understood to contain the image charge of the RD ion (see Supplementary Fig 3). By varying (i) the initial translational energy along the surface normal, and (ii) the initial orientation of the incident molecule (see Fig 3A, shown as the surface approaching the molecule), the calculations reproduced the three outcomes observed in the experiment: the non-reactive INTACT pathway, and the bond-selective CRACK and SPLIT pathways, with a threshold of 12 eV for CRACK, and 14 eV for SPLIT. Most notably the computed reaction probabilities were found to reproduce the experimental trend, as shown in Fig 2B and Supplementary Fig 4, thereby validating the collision dynamics unveiled by the MD.

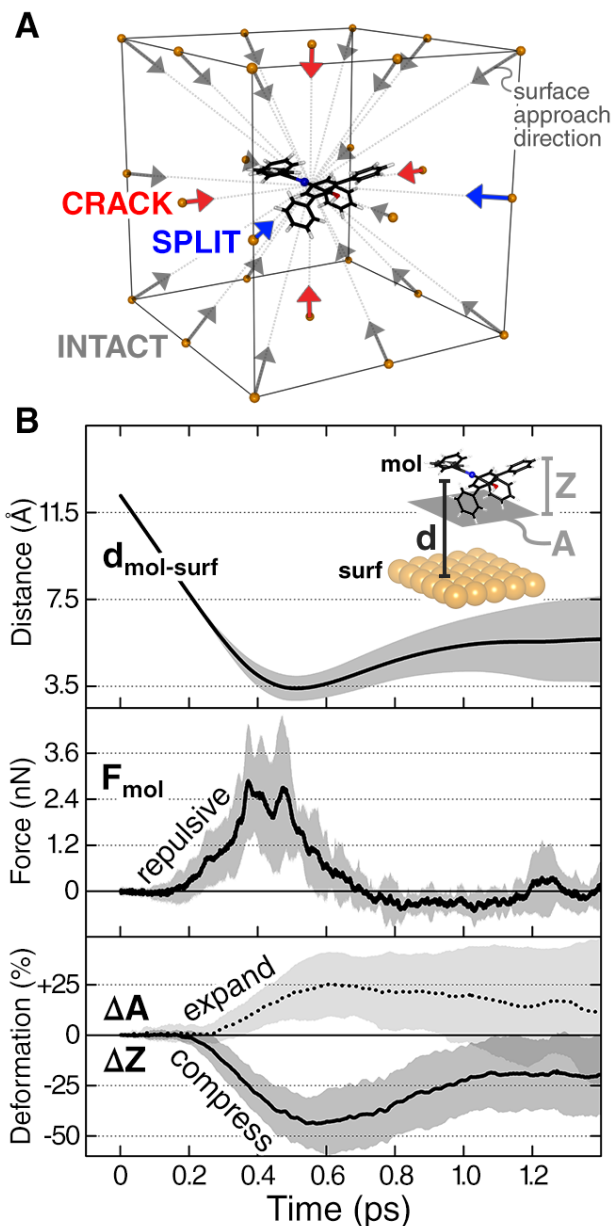


**Fig. 3. | Computed dynamics of RD-Cu(100) collision with varied initial geometries. A.** Schematics of different initial RD geometries simulated for 15 eV collision energy, illustrated here as the surface approaching the molecule (the arrows mark the surface normal). The red and blue arrows indicate initial geometries that give CRACK and SPLIT outcomes respectively; and the grey arrows, for INTACT. **B.** Time-dependent quantities of RD averaged between all trajectories with different initial geometries: the molecule-surface distance ( $d_{\text{mol-surf}}$ ), the stopping force exerted by the surface on RD ( $F_{\text{mol}}$ ), the change in RD cross-section along the surface plane direction ( $\Delta A$ , dotted line), and the compression of RD along the surface normal ( $\Delta Z$ , solid line). The data is shown for 15 eV incident energy whereby the stopping force went up to  $\sim 2.4$  nN for  $\sim 125$  fs, compressing the *entire* molecule by  $\sim 45\%$  and expanding its area by  $\sim 25\%$  laterally. The shaded area gives the standard deviation between all trajectories.

The collision dynamics for all three pathways in general showed the molecule to be compressed onto surface due to the mechanical impulse from the molecule-surface impact. As shown in Fig 3B, the stopping force exerted by the surface on the incident molecule was computed to be operative in the nano-Newton regime at sub-picosecond timescale (see also Supplementary Fig 5). This impulse is understood to move the system to a region on the potential energy surface along the compression coordinate. For the reactive CRACK and SPLIT outcome, the system was impulsively propelled to a transition state en route to a product potential well.

The computed dynamics for CRACK and SPLIT show the collision-induced compression precedes the bond-selective dissociation (see Fig 4 and Supplementary Movie 1 and 2). The compression bends a specific C-N bond (i.e. C-N(AC) in CRACK and C-N(AL) in SPLIT) prior to its dissociation (see bottom panels of Fig 4). This C-N bond bending was noted to modify the local geometry of the C-atom from a trigonal planar ( $sp^2$  C-atom) to a trigonal pyramidal ( $sp^3$  C-atom), in effect converting a p-orbital into a  $sp^3$ -hybridized C-dangling bond. Upon contact with the surface, this bent C-N bond breaks, and concurrently a new C-Cu bond forms, indicating a reactive event whose transition state is stabilized by the formation of a new bond (36). In both pathways, the trajectory shows the C-N bond to dissociate in a single attempt, evidencing a *direct* energy transfer from the translational energy to the reaction coordinate.

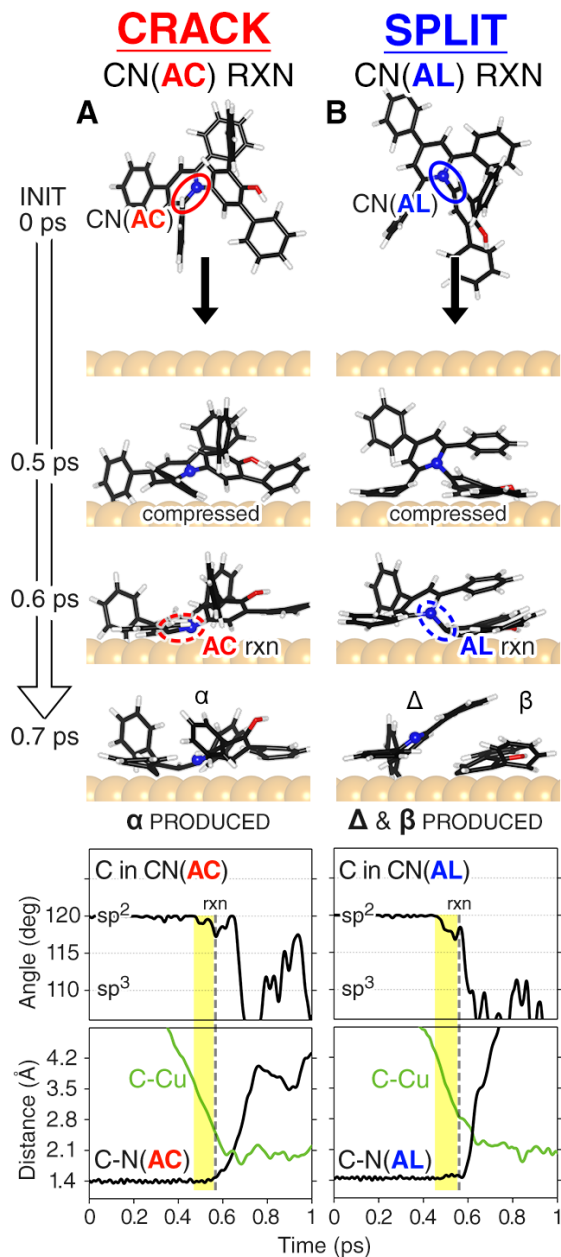


**Fig. 4. | Reactive trajectories for CRACK and SPLIT in RD-Cu(100) collision.** Time-dependent snapshots of the CRACK pathway in **A** and SPLIT in **B**. The trajectories shown are for the minimum translational energy required to give a reactive outcome: 12 eV for the CRACK pathway and 14 eV for SPLIT. The bottom panels show time-dependent quantities of RD: the angle gives the average angle formed between the C-atom and two of its neighboring atoms, which checks whether the C-atom in the C-N bond is in a  $sp^2$ - or  $sp^3$ -like geometry; and the distance gives the separation between the C- and N-atom in the reacting C-N bond as a black line, and the separation between the C-atom of the reacting C-N bond and the nearest Cu-atom as a green line. The yellow area marks the region where the compression from the collision bends the C-N bonds; the dashed line marks the beginning of the C-N rupture.

The preferential breaking of the C-N bond for the bond-selective CRACK and SPLIT pathways was understood to be due to its pronounced reactivity, which we attribute to two factors: (i) the destabilization due to C-N bending, and (ii) the C-N antibonding orbital being the lowest unoccupied molecular orbital (LUMO) of RD (see Supplementary Fig 6). The importance of these two factors were suggested by the correlation between C-N dissociation, and the charge flow from the surface to the LUMO of the compressed RD (i.e. RD with bent C-N bonds) (see Supplementary Fig 7). Similar to mechanism proposed for C-H dissociation of benzene on Cu-surface (37), we expect the orbital mixing caused by the C-N bond-bending increases the propensity of the RD LUMO to hybridize, and form a bond with the surface. The proposed mechanism in which bond-bending alters the electronic structure of a reacting molecule is noted to be topical in mechanochemistry (28, 29).

Finally, to address the possibility of the hyperthermal collision giving a chemical reaction via a precursor state of RD, we examined the minimum energy pathway (MEP) of an adsorbed RD. We consider this alternative pathway because an incident RD that had failed to react upon its first collision would have its energy increasingly equipartitioned among all its degrees of freedom while being trapped on surface, allowing the system to search for the MEP to react. The computed barrier along the MEP from an adsorbed RD to give an  $\alpha$ -fragment was 1.23 eV, and to give a  $\beta$ - and  $\Delta$ -fragments, 0.28 eV (see Supplementary Fig 8). The MEP barrier thus predict a reactive outcome dominated by the  $\beta$ - and  $\Delta$ -fragments, in agreement with the thermal reaction experiment of adsorbed RD at  $\sim 350$  K, which only gave  $\beta$ - and  $\Delta$ -fragments as products. The hyperthermal collision clearly deviates from the MEP prediction since the  $\alpha$ -fragment was the major product, thereby ruling out reactions via precursor state.

In conclusion, we have reported here the first observation of a bond-selective reaction from a hyperthermal collision of a polyatomic ion with a metal surface. The collision gave a mechanical impulse that compresses the incident molecule, causing a specific chemical bond to be activated. From a fundamental standpoint, we expect the collision-induced molecular compression described here to be a general phenomenon across surfaces with similar stiffness; and we expect such mechanism to play a central role in surface-induced dissociation experiments in tandem mass spectroscopy (13–17). The experimental method described here provides a new general tool to study and apply compressive mechanochemistry for any molecules that can be electrosprayed (27). Here the compression is operative on the *entire* molecule, instead of locally (38), for subpicoseconds, instead of permanently (29), thereby opening a new avenue to explore *impulsive* mechanochemistry. Additionally, the method described here offers new scalable method to non-thermally activate molecules to generate species that are inaccessible from conventional thermochemistry (12, 27).

## **METHODS**

### **Experiment**

A home-built Electrospray Ion-beam Deposition (ES-IBD) apparatus, described in detail in elsewhere (27), was used to collide the Reichardt's Dye (RD) ion onto the Cu-surface. A dilute solution ( $\sim 10^{-4}$  M) of RD (Sigma-Aldrich, 90%) in 3:1 ethanol:water was electrosprayed in positive-mode to generate a beam of monoprotonated  $[\text{RD}+\text{H}]^{1+}$  in the gas-phase. The species in the ion beam ( $m/z = 552$ ) was mass-selected before its beam energy ( $E_{\text{BEAM}}$ ) was characterized by measuring the ion-beam current impinging on an electrode as a function of retarding voltage applied to a grid placed in front of that electrode.

For deposition, the ion-beam was transmitted to an ultra-high vacuum (UHV) chamber ( $P \approx 10^{-10}$  mbar) and aimed at normal incident angle onto a clean single-crystal Cu(100) surface held at room temperature. A retarding potential ( $V_{\text{DECEL}}$ ) was applied on the Cu-surface to decelerate the incoming ions which controlled the molecule-surface collision energy ( $E_{\text{COL}} = E_{\text{BEAM}} - eV_{\text{DECEL}}$ ,  $e$  is elementary charge). Prior to the deposition, the Cu(100) surface was cleaned by repeated cycles of Ar-ion sputtering with 1 keV beam energy and thermal annealing at  $\sim 600$  K in the UHV environment. After the deposition, the surface was brought to a low-temperature scanning tunnelling microscope (Omicron Fermi SPM), where the surface was scanned at 11 K.

#### Data Analysis: Event Probability

To find the probability for all three reported pathways: INTACT, CRACK and SPLIT, we determined the coverage for the final state species of each pathways. The probability for a pathway X was determined by dividing counted species  $N_X$  by the total coverage  $N_{\text{TOT}}$ , the sum of  $N_{\text{INTACT}}$ ,  $N_{\text{CRACK}}$  and  $N_{\text{SPLIT}}$ . For the SPLIT pathway,  $N_{\text{SPLIT}}$  refers to the average of number of  $\beta$ - and  $\Delta$ -fragments, which were both found in equal quantities at all collision energies. On average, we made  $\sim 300$  observations (i.e.  $N_{\text{TOT}}$ ) for every collision energy. Some ambiguous species were excluded from the analysis; this refers to species that were in close proximity to one another, or species adsorbed at the step edges. The exclusion of such species did not bias the probabilities reported in Fig 2, since similar populations ( $\sim 10\%$ ) of such species were found for every collision energy. We expect these species to possess the same relative populations of species as the adsorbates observed on the surface terrace.

We estimated that there is no significant scattering of molecules to the gas phase upon collision since most of the incident molecules remained on the surface, even at 50 eV collision energy. This is evidenced by the good agreement between the total deposited charge and the observed coverage, as shown in Extended Data Fig 1. Typically we deposited a total charge of  $\sim 50$  pAh (1 pAh = 1 picoampere



hour) on a deposition area of  $12.5 \text{ mm}^2$  for which we expect a density of  $\sim 225$  molecules in a  $50 \times 50 \text{ nm}^2$  area. The observed high sticking probability for large polyatomic ions at 50 eV collision energy is consistent with that reported in the literature<sup>13</sup>.

### Data Analysis: Threshold Energies

To fit the experimental data that we inferred to be due to an impulsive collision dynamics, we constructed a mathematical model inspired by the Sudden Vector Projection method that has been applied to model impulsive dynamics in the gas phase and on surfaces (19). For every reactive pathway, i.e. CRACK and SPLIT, we postulated:

- (1) Unique, non-overlapping reaction coordinate (RC) oriented at a specific axis from the molecule, as illustrated in Extended Data Fig 2.
- (2) Each RC-axis possesses a unique threshold energy ( $E_T$ ) for which the reaction would occur if energy supplied along this coordinate is larger than  $E_T$ .

In the context of a surface approaching the molecule as shown in Extended Data Fig 2, the kinetic energy supplied along a specific RC ( $E_{RC}$ ) was determined by projecting the surface-approach-velocity vector onto the direction vector of the RC, which leads to:

$$E_{RC} = E_{COL} \cos^2 \varphi$$

where  $E_{COL}$  is the kinetic energy of the molecule approaching the surface at normal incident angle, and  $\varphi$  is the angle between the surface-approach-velocity vector and the RC-vector. We limit the domain of  $\varphi$  to  $[-\pi/2, \pi/2]$ , thereby only considering approach angles that point towards the hemisphere whose axis is the RC-vector (illustrated in Extended Data Fig 2). This expression thus allows premise (2) to be written mathematically as:

$$p_{\text{RXN}}(E_{\text{COL}}, \varphi) = \begin{cases} 1 & \text{for } E_{\text{RC}} \geq E_{\text{T}} \\ 0 & \text{for } E_{\text{RC}} < E_{\text{T}} \end{cases}$$

For gaseous molecules impacting on the surface at random orientation as in the experiment, we assume an equiprobable distribution of  $\varphi$ , expressed mathematically as:

$$f(\varphi) = \frac{1}{\pi}$$

The cumulative probability at a given  $E_{\text{COL}}$  can therefore be written as:

$$P_{\text{RXN}}(E_{\text{COL}}) = \int_{-\pi/2}^{\pi/2} f(\varphi) p_{\text{RXN}}(E_{\text{COL}}, \varphi) d\varphi$$

Since  $p_{\text{RXN}}$  is unity only for a range of  $\varphi$  that gives  $E_{\text{RC}} \geq E_{\text{T}}$ , we demarcate the maximum range of  $\varphi$  by a constant  $\varphi_{\text{max}}$ . As a result, the expression simplifies to:

$$P_{\text{RXN}}(E_{\text{COL}}) = \frac{1}{\pi} \int_{-\varphi_{\text{max}}}^{\varphi_{\text{max}}} d\varphi = \frac{2\varphi_{\text{max}}}{\pi}$$

where:

$$\varphi_{\text{max}}(E_{\text{COL}}) = \cos^{-1} \sqrt{\frac{E_{\text{T}}}{E_{\text{COL}}}}$$

which gives the cumulative probability for one reaction coordinate at a given  $E_{\text{COL}}$  as:

$$P_{\text{RXN}}(E_{\text{COL}}) = \frac{2}{\pi} \cos^{-1} \sqrt{\frac{E_{\text{T}}}{E_{\text{COL}}}}$$

Each collision can give multiple outcomes, and each outcome can have a number of reaction coordinates. Thus we impose a normalization condition where the sum of probability for all pathways, both reactive and non-reactive, at a specific  $E_{\text{COL}}$  to be equal to 1, expressed as:

$$P_{\text{INTACT}} + P_{\text{CRACK}} + P_{\text{SPLIT}} = 1$$

We enforce this condition by scaling the event probability by a factor  $P_{\text{SAT},X}$  that is unique for each pathway, and independent from  $E_{\text{COL}}$ , thereby yielding the final expression for pathway X (X could be INTACT, CRACK or SPLIT):

$$P_X(E_{\text{COL}}) = P_{\text{SAT},X} \cos^{-1} \sqrt{\frac{E_{T,X}}{E_{\text{COL}}}} \quad \dots (1)$$

where  $P_{\text{SAT},X}$  is the saturation reaction probability observed at high energy.

To account for the spread in collision energy as in the experiment, we perform a convolution integral in which we replaced the exact  $E_{\text{COL}}$  by a Gaussian distribution centered at  $\bar{E}_{\text{COL}}$  with a standard deviation of  $\Delta E$ , yielding the expression of pathway X:

$$P_{\text{RXN},X}(\bar{E}_{\text{COL}}) = \int_0^\infty \frac{1}{\sqrt{2\pi} \Delta E} \exp\left(-\frac{(E_{\text{COL}} - \bar{E}_{\text{COL}})^2}{2\Delta E^2}\right) P_{\text{SAT},X} \cos^{-1} \sqrt{\frac{E_{T,X}}{E_{\text{COL}}}} dE_{\text{COL}} \quad (2)$$

The equations above were numerically fitted to the experimental results and to the ab-initio calculation results, both yielding good agreement as shown in Extended Data Fig 4. Fitting of Eq (2) to the experiment yielded:  $E_{T,\text{CRACK}} = 5.98$  eV,  $E_{T,\text{SPLIT}} = 9.48$  eV,  $P_{\text{SAT},\text{CRACK}} = 0.44$ ,  $P_{\text{SAT},\text{SPLIT}} = 0.35$ ; while fitting Eq (1) to the ab-initio MD results yielded:  $E_{T,\text{CRACK}} = 11.22$  eV,  $E_{T,\text{SPLIT}} = 14.01$  eV,  $P_{\text{SAT},\text{CRACK}} = 0.38$ ,  $P_{\text{SAT},\text{SPLIT}} = 0.39$ . Here the discrepancy between the threshold energies from experiment and ab-initio results can be accounted for by the contribution of Coulomb energy gained due to a molecular ion approaching its image charge missing in the abscissa of Fig 2B and Extended Data Fig 4 (in the EXPT+FIT panel). We estimated the energy to be  $\sim 3$  eV to be added to the kinetic energy for a point charge approaching its image charge from infinity to its closest-approach distance with the surface (i.e.  $\sim 2.5$  Å above the image plane). This correction modified the experimental  $E_T$  to 9 eV for CRACK, and 12 eV for SPLIT. Furthermore, the threshold energies from ab-initio calculations could be offset by 0.5 - 3.0 eV due to errors in estimating electrostatic interactions with the surface caused by the limited supercell size (57) used in the MD calculations.

### Theory: Structure Relaxations, STM Simulations, and Minimum Energy Paths

Density Functional Theory (DFT), STM and Nudged Elastic Band (NEB) (39, 40) calculations were performed with the plane wave-pseudopotential package Quantum ESPRESSO (41), using Ultrasoft pseudopotentials (42) with a wave function (charge) kinetic energy cutoff of 408 eV (4080 eV) and a GGA-PBE (43) exchange-correlation functional. The rVV10 (44) self-consistent van der Waals interaction was included. The Brillouin-zone was sampled with the  $\mathbf{k} = \Gamma$  point, with a Methfessel-Paxton (45) smearing of 0.27 eV. The Cu(100) surface was modeled with a periodically repeated slab of three layers, with a vacuum gap between the adsorbed molecule and the bottom layer of the slab replica of  $\sim 10$  Å. Only forces on molecule atoms and surface atoms belonging to the first two layers were allowed to relax, up to 0.026 eV/Å.

STM simulations were performed by calculating the integrated local density of states (ILDOS) within the Tersoff-Hamann method (46). STM simulations of the intact molecule,  $\alpha$ -fragment,  $\Delta$ -fragment, and  $\beta$ -fragment decorated with a Cu-adatom were obtained at a constant current using the LEV00 package v3.4 (see ref (47)).

NEB calculations are shown in Supplementary Fig 8. In the upper panel we present the Minimum Energy Path (MEP) corresponding to the CRACK reaction of the intact molecule leading to the  $\alpha$ -fragment (energy barrier 1.23 eV). In the lower panel, the MEP for the SPLIT reaction to give a  $\beta$ - and  $\Delta$ -fragments, obtaining a much lower barrier, 0.28 eV. These very different barrier values are compatible with the experimental observations of SPLIT products in the thermal reaction, whereas the CRACK product is observed only in hyperthermal reaction. Note also that while the  $\alpha$ -fragment is 0.4 eV less stable than the intact molecule, the  $\beta$ - and  $\Delta$ -

fragments are 0.3 eV more stable. In both NEBs, the state in the reaction coordinate  $R_c=1$  corresponds to the intact molecule in Figure 1B (left panel); the  $R_c=5$  state in Supplementary Fig 8 (upper panel) to the  $\alpha$ -fragment in Figure 1B (central panel) while the  $R_c=7$  state in Supplementary Fig 8 (lower panel) to the  $\beta$ - and  $\Delta$ -fragments in Figure 1B (right panel) without adatom attached to the  $\beta$ .

### Theory: Molecular Dynamics

Plane-wave DFT calculations as implemented in Vienna Ab-initio Simulation Package (VASP 5.4.4) (ref (48, 49)) were used to model the molecule-surface collision. The calculation used the projector augmented wave method (42, 50), Perdew-Burke-Ernzerhof (PBE) functional (43) and Grimme's semiempirical correction for van der Waals interaction (DFT-D3) (ref (51)). The Born-Oppenheimer molecular dynamics (MD) and barrier height calculations were performed at the  $\Gamma$ -point, with a cutoff energy at 400 eV. The Cu(100) surface was modeled as a  $(9 \times 8)$  slab with four layers of atoms, where the lowest layer was frozen; and a vacuum gap of 25 Å. The projected-Density-of-States (pDOS) calculations employed a Gaussian smearing with  $\sigma = 0.25$  eV. The molecular models and the charge density were visualized using the VESTA software (52).

The MD calculations were performed to simulate the collision dynamics between RD and the Cu(100) surface on the ground potential energy surface. The initial state was a hydrogenated RD with its center-of-mass placed 12 Å above the first layer of the Cu-slab. Each atom in the molecule was given an identical velocity along the surface normal towards the Cu-slab, which sets the center-of-mass translational energy to be the experimental collision energy ( $E_{COL}$ ). Additionally all atoms in the molecule and in the Cu-slab were initialized with random velocities sampled from a Boltzmann distribution at 298 K. The MD simulations were performed with a

time-step of 0.5 fs as a microcanonical system that conserved the number of atoms (N), the volume of the supercell (V), and the total energy of the system (E).

The barrier height in the ground potential energy surface for the dehydrogenation of a singly hydrogenated RD on surface was obtained by climbing-image NEB calculations (39, 40). The calculations were performed with at least 5 images between the initial and the final state. The band was relaxed until the forces orthogonal to the reaction coordinate were lower than 0.02 eV/Å.

### Theory: Gas-Phase Calculations

The structure of gaseous RD monocation was computed using ORCA (53), employing PBE functional (43), and Grimme's DFT-D3 Van der Waals correction (51). The calculation was performed using ma-def2-SVP basis sets (54, 55), and with the auxiliary basis sets chosen automatically (56).

## **REFERENCES**

1. S. T. Ceyer, New Mechanisms for Chemistry at Surfaces. *Science*. **249**, 133–139 (1990).
2. H. Hou, S. J. Gulding, C. T. Rettner, A. M. Wodtke, D. J. Auerbach, The Stereodynamics of a Gas-Surface Reaction. *Science*. **277**, 80–82 (1997).
3. R. D. Beck, *et al.*, Vibrational Mode-Specific Reaction of Methane on a Nickel Surface. *Science*. **302**, 98–100 (2003).
4. R. R. Smith, D. R. Killelea, D. F. DelSesto, A. L. Utz, Preference for Vibrational over Translational Energy in a Gas-Surface Reaction. *Science*. **304**, 992–995 (2004).
5. D. R. Killelea, V. L. Campbell, N. S. Shuman, A. L. Utz, Bond-Selective Control of a Heterogeneously Catalyzed Reaction. *Science*. **319**, 790–793 (2008).
6. B. L. Yoder, R. Bisson, R. D. Beck, Steric Effects in the Chemisorption of Vibrationally Excited Methane on Ni(100). *Science*. **329**, 553–556 (2010).
7. L. Chen, H. Ueta, R. Bisson, R. D. Beck, Vibrationally bond-selected chemisorption of

- methane isotopologues on Pt(111) studied by reflection absorption infrared spectroscopy. *Faraday Discuss.* **157**, 285–295 (2012).
8. X. J. Shen, A. Lozano, W. Dong, H. F. Busnengo, X. H. Yan, Towards Bond Selective Chemistry from First Principles: Methane on Metal Surfaces. *Phys. Rev. Lett.* **112**, 46101 (2014).
  9. B. Jiang, M. Yang, D. Xie, H. Guo, Quantum dynamics of polyatomic dissociative chemisorption on transition metal surfaces: mode specificity and bond selectivity. *Chem. Soc. Rev.* **45**, 3621–3640 (2016).
  10. D. C. Jacobs, Reactive Collisions Of Hyperthermal Energy Molecular Ions With Solid Surfaces. *Annu. Rev. Phys. Chem.* **53**, 379–407 (2002).
  11. J. V Barth, G. Costantini, K. Kern, Engineering atomic and molecular nanostructures at surfaces. *Nature* **437**, 671 (2005).
  12. G. Dubey, *et al.*, Chemical Modification of Graphene via Hyperthermal Molecular Reaction. *J. Am. Chem. Soc.* **136**, 13482–13485 (2014).
  13. A. R. Dongré, Á. Somogyi, V. H. Wysocki, Surface-induced Dissociation: An Effective Tool to Probe Structure, Energetics and Fragmentation Mechanisms of Protonated Peptides. *J. Mass Spectrom.* **31**, 339–350 (1996).
  14. V. Grill, J. Shen, C. Evans, R. G. Cooks, Collisions of ions with surfaces at chemically relevant energies: Instrumentation and phenomena. *Rev. Sci. Instrum.* **72**, 3149–3179 (2001).
  15. J. Laskin, T. H. Bailey, J. H. Futrell, Shattering of Peptide Ions on Self-Assembled Monolayer Surfaces. *J. Am. Chem. Soc.* **125**, 1625–1632 (2003).
  16. X. Ma, M. Zhou, V. H. Wysocki, Surface Induced Dissociation Yields Quaternary Substructure of Refractory Noncovalent Phosphorylase B and Glutamate Dehydrogenase Complexes. *J. Am. Soc. Mass Spectrom.* **25**, 368–379 (2014).
  17. S. R. Harvey, *et al.*, Relative interfacial cleavage energetics of protein complexes revealed by surface collisions. *Proc. Natl. Acad. Sci.* **116**, 8143–8148 (2019).
  18. F. F. Crim, Chemical dynamics of vibrationally excited molecules: Controlling reactions in gases and on surfaces. *Proc. Natl. Acad. Sci.* **105**, 12654–12661 (2008).
  19. H. Guo, B. Jiang, The Sudden Vector Projection Model for Reactivity: Mode Specificity and Bond Selectivity Made Simple. *Acc. Chem. Res.* **47**, 3679–3685 (2014).
  20. B. D. Kay, T. D. Raymond, M. E. Coltrin, Observation of Direct Multiquantum Vibrational Excitation in Gas-Surface Scattering: NH<sub>3</sub> on Au(111). *Phys. Rev. Lett.* **59**, 2792–2794 (1987).
  21. K. Golibrzuch, *et al.*, Observation of Translation-to-Vibration Excitation in Acetylene Scattering from Au(111): A REMPI Based Approach. *Zeitschrift für Phys. Chemie* **229**, 1929 (2015).
  22. J. A. Burroughs, S. B. Wainhaus, L. Hanley, Impulsive Excitation of Cr(CO)<sub>6</sub><sup>+</sup> during

- Surface-Induced Dissociation at Organic Monolayers. *J. Phys. Chem.* **98**, 10913–10919 (1994).
23. R. D. Beck, J. Rockenberger, P. Weis, M. M. Kappes, Fragmentation of C<sub>60</sub> and higher fullerenes by surface impact. *J. Chem. Phys.* **104**, 3638–3650 (1996).
  24. W. R. Koppers, *et al.*, Dissociation of polyatomic ions at surfaces: The influence of mechanical and electronic energy transfer. *Phys. Rev. B* **53**, 11207–11210 (1996).
  25. J. R. Morris, G. Kim, T. L. O. Barstis, R. Mitra, D. C. Jacobs, Dynamics of dissociative scattering: Hyperthermal energy collisions of state-selected OCS<sup>+</sup> on Ag(111). *J. Chem. Phys.* **107**, 6448–6459 (1997).
  26. Y. Yao, P. Shushkov, T. F. Miller, K. P. Giapis, Direct dioxygen evolution in collisions of carbon dioxide with surfaces. *Nat. Commun.* **10**, 2294 (2019).
  27. S. Rauschenbach, M. Ternes, L. Harnau, K. Kern, Mass Spectrometry as a Preparative Tool for the Surface Science of Large Molecules. *Annu. Rev. Anal. Chem.* **9**, 473–498 (2016).
  28. J. J. Gilman, Mechanochemistry. *Science*. **274**, 65 (1996).
  29. H. Yan, *et al.*, Sterically controlled mechanochemistry under hydrostatic pressure. *Nature* **554**, 505 (2018).
  30. E. Kolodney, A. Amirav, R. Elber, R. B. Gerber, Energy transfer and dissociation in collisions of I<sub>2</sub> with MgO(100). *Chem. Phys. Lett.* **111**, 366–371 (1984).
  31. H. A. Michelsen, C. T. Rettner, D. J. Auerbach, R. N. Zare, Effect of rotation on the translational and vibrational energy dependence of the dissociative adsorption of D<sub>2</sub> on Cu(111). *J. Chem. Phys.* **98**, 8294–8307 (1993).
  32. R. D. Levine, *Molecular Reaction Dynamics* (Cambridge University Press, 2005) <https://doi.org/DOI: 10.1017/CBO9780511614125>.
  33. J. C. Polanyi, R. J. Wolf, Dynamics of Simple Gas-Surface Interaction. I. Rotationally Inelastic Collisions at Smooth Surfaces. *Berichte der Bunsengesellschaft für Phys. Chemie* **86**, 356–361 (1982).
  34. J. C. Polanyi, R. J. Wolf, Dynamics of simple gas–surface interaction. II. Rotationally inelastic collisions at rigid and moving surfaces. *J. Chem. Phys.* **82**, 1555–1566 (1985).
  35. K. D. Rendulic, A. Winkler, Adsorption and desorption dynamics as seen through molecular beam techniques. *Surf. Sci.* **299–300**, 261–276 (1994).
  36. L. Leung, T. Lim, Z. Ning, J. C. Polanyi, Localized Reaction at a Smooth Metal Surface: p-Diodobenzene at Cu(110). *J. Am. Chem. Soc.* **134**, 9320–9326 (2012).
  37. H. Lesnard, M.-L. Bocquet, N. Lorente, Dehydrogenation of Aromatic Molecules under a Scanning Tunneling Microscope: Pathways and Inelastic Spectroscopy Simulations. *J. Am. Chem. Soc.* **129**, 4298–4305 (2007).
  38. J. N. Ladenthin, *et al.*, Force-induced tautomerization in a single molecule. *Nat. Chem.* **8**,



- 935 (2016).
39. H. Jónsson, G. Mills, K. W. Jacobsen, “Nudged elastic band method for finding minimum energy paths of transitions” in *‘Nudged Elastic Band Method for Finding Minimum Energy Paths of Transitions’* in “*Classical and Quantum Dynamics in Condensed Phase Simulations*,” B. J. Berne, G. Ciccotti, D. F. Coker, Eds. (World Scientific, 1998), p. 385.
  40. G. Henkelman, B. P. Uberuaga, H. Jónsson, A climbing image nudged elastic band method for finding saddle points and minimum energy paths. *J. Chem. Phys.* **113**, 9901–9904 (2000).
  41. P. Giannozzi, *et al.*, QUANTUM ESPRESSO: a modular and open-source software project for quantum simulations of materials. *J. Phys. Condens. Matter* **21**, 395502 (2009).
  42. G. Kresse, D. Joubert, From ultrasoft pseudopotentials to the projector augmented-wave method. *Phys. Rev. B* **59**, 1758–1775 (1999).
  43. J. P. Perdew, K. Burke, M. Ernzerhof, Generalized Gradient Approximation Made Simple. *Phys. Rev. Lett.* **77**, 3865–3868 (1996).
  44. R. Sabatini, T. Gorni, S. de Gironcoli, Nonlocal van der Waals density functional made simple and efficient. *Phys. Rev. B* **87**, 41108 (2013).
  45. M. Methfessel, A. T. Paxton, High-precision sampling for Brillouin-zone integration in metals. *Phys. Rev. B* **40**, 3616–3621 (1989).
  46. J. Tersoff, D. R. Hamann, Theory of the scanning tunneling microscope. *Phys. Rev. B* **31**, 805–813 (1985).
  47. L. N. Kantorovich, User-friendly visualisation program for ab initio DFT codes VASP, SIESTA, QE and QUICKSTEP (1996).
  48. G. Kresse, J. Hafner, Ab initio molecular dynamics for liquid metals. *Phys. Rev. B* **47**, 558–561 (1993).
  49. G. Kresse, J. Furthmüller, Efficient iterative schemes for ab initio total-energy calculations using a plane-wave basis set. *Phys. Rev. B* **54**, 11169–11186 (1996).
  50. P. E. Blöchl, Projector augmented-wave method. *Phys. Rev. B* **50**, 17953–17979 (1994).
  51. S. Grimme, J. Antony, S. Ehrlich, H. Krieg, A consistent and accurate ab initio parametrization of density functional dispersion correction (DFT-D) for the 94 elements H-Pu. *J. Chem. Phys.* **132**, 154104 (2010).
  52. K. Momma, F. Izumi, VESTA3 for three-dimensional visualization of crystal, volumetric and morphology data. *J. Appl. Crystallogr.* **44**, 1272–1276 (2011).
  53. F. Neese, The ORCA program system. *Wiley Interdiscip. Rev. Comput. Mol. Sci.* **2**, 73–78 (2012).
  54. F. Weigend, R. Ahlrichs, Balanced basis sets of split valence, triple zeta valence and quadruple zeta valence quality for H to Rn: Design and assessment of accuracy. *Phys. Chem. Chem. Phys.* **7**, 3297–3305 (2005).

55. J. Zheng, X. Xu, D. G. Truhlar, Minimally augmented Karlsruhe basis sets. *Theor. Chem. Acc.* **128**, 295–305 (2011).
56. G. L. Stoychev, A. A. Auer, F. Neese, Automatic Generation of Auxiliary Basis Sets. *J. Chem. Theory Comput.* **13**, 554–562 (2017).
57. Geada, I. L., Ramezani-Dakhel, H., Jamil, T., Sulpizi, M. & Heinz, H. Insight into induced charges at metal surfaces and biointerfaces using a polarizable Lennard–Jones potential. *Nat. Commun.* **9**, 716 (2018).

## **DATA AVAILABILITY**

The authors declare that the data supporting the findings of this study are available from the corresponding author upon request.

## **ACKNOWLEDGEMENTS**

This work is dedicated to the memory Prof. Alessandro De Vita. We thank Rico Gutzler, John Polanyi, Claire Vallance, and Mark Brouard for fruitful discussions. Calculations were performed on the supercomputers at Max-Planck Computing and Data Facility in Garching. The research is funded by the Max-Planck Society. K.A. thanks Alexander von Humboldt Foundation for financial support. Via our membership of the UK's HEC Materials Chemistry Consortium, which is funded by EPSRC (EP/L000202, EP/R029431), this work used the ARCHER UK National Supercomputing Service (<http://www.archer.ac.uk>) and the UK Materials and Molecular Modelling Hub for computational resources, MMM Hub, which is partially funded by EPSRC (EP/P020194).

## **AUTHOR CONTRIBUTIONS**

S.R. designed and supervised the project. S.R., S.A., K.K., U.S. planned experiments. L.K., S.R., T.M., G.R. performed the experiments. L.K., S.R. H.O., K.A., S.A., A.B. analyzed experimental

data. U.S., T.M., A.P., and M.D. performed chemical analysis measurement. K.A., M.S., A.F. performed the DFT calculations.

### **COMPETING INTERESTS**

The authors declare no competing financial interests.

## SUPPORTING INFORMATION

### **Fast Molecular Compression by Hyperthermal Collision Gives Bond-Selective Mechanochemistry**

Lukas Krumbein<sup>†,1</sup>, Kelvin Anggara<sup>†,1</sup>, Martina Stella<sup>2</sup>, Tomasz Michnowicz<sup>1</sup>, Hannah Ochner<sup>1</sup>, Sabine Abb<sup>1</sup>, Gordon Rinke<sup>1</sup>, André Portz<sup>3</sup>, Michael Dürr<sup>3</sup>, Uta Schlickum<sup>1,4</sup>, Andrew Baldwin<sup>5</sup>, Andrea Floris<sup>6</sup>,  
Klaus Kern<sup>1,7</sup>, Stephan Rauschenbach<sup>1,5\*</sup>

<sup>1</sup>*Max-Planck-Institut für Festkörperforschung, Heisenbergstrasse 1, DE-70569 Stuttgart, Germany.*

<sup>2</sup>*Department of Materials, Royal School of Mines, Imperial College London, Exhibition Road, London, SW7 2A2, United Kingdom.*

<sup>3</sup>*Institut für Angewandte Physik, Justus-Liebig-Universität Giessen, Heinrich-Buff-Ring 16, DE-35392 Giessen, Germany.*

<sup>4</sup>*Institut für Angewandte Physik, Technische Universität Braunschweig, Mendelssohnstrasse 2, DE-38106 Braunschweig, Germany.*

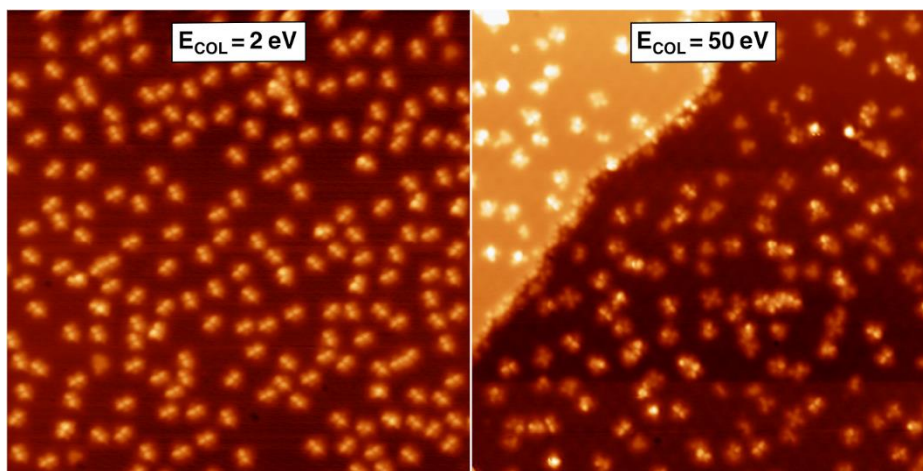
<sup>5</sup>*Chemistry Research Laboratory, Department of Chemistry, University of Oxford, 12 Mansfield Road, Oxford, OX1 3TA, United Kingdom.*

<sup>6</sup>*School of Chemistry, University of Lincoln, Brayford Pool, LN6 7TS, Lincoln, United Kingdom.*

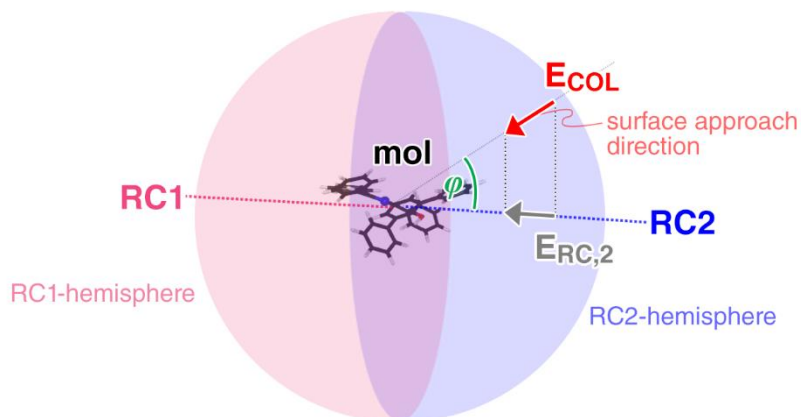
<sup>7</sup>*Institut de Physique, École Polytechnique Fédérale de Lausanne, Laussane, CH-1015, Switzerland.*

\*Correspondence to: stephan.rauschenbach@chem.ox.ac.uk

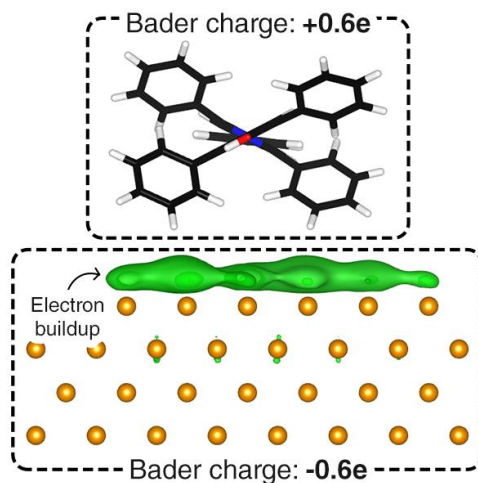
<sup>†</sup>equal contributions

**SUPPORTING INFORMATION**

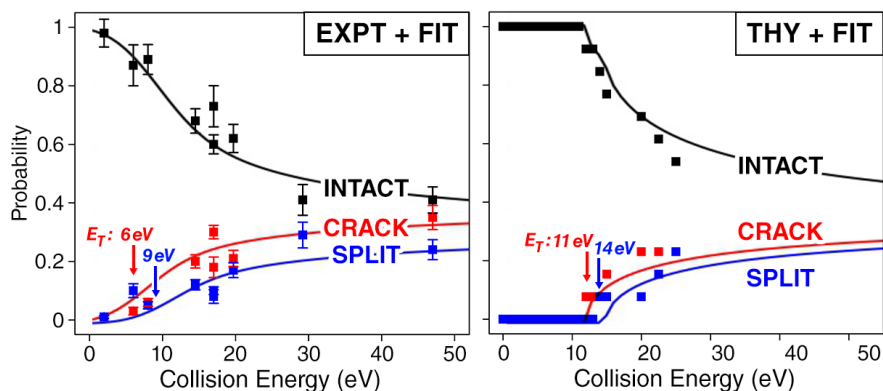
**Supporting Information Fig S1. Large-scale image of RD-decorated Cu-surface.** Representative large-scale images ( $50 \times 50 \text{ nm}^2$ ) of RD-decorated surface at two different collision energies ( $E_{\text{COL}}$ ). In both cases, the coverage measured from the integrated ion flux was 40 pAh, which corresponds to  $\sim 180$  molecules per  $50 \times 50 \text{ nm}^2$ . The difference in surface coverage between these two extreme cases was found to be below  $\sim 20\%$ , which can be attributed to anisotropic beam-profile on the surface.



**Supporting Information Fig S2. Illustration of collision model.** The outcome of collision is determined by the magnitude of the surface approach vector projected into the reaction-coordinate (RC) – here exemplified by RC1 (in pink) and RC2 (in blue), both shown with their corresponding hemisphere. An example of collision event is defined by an approach vector with a kinetic energy ( $E_{COL}$ ), which forms an angle  $\varphi$  (shown in green) with the RC-vector in one of the hemispheres. The projection of the approach vector to the RC-vector was used to compute the kinetic energy that flows along the RC ( $E_{RC}$ ).



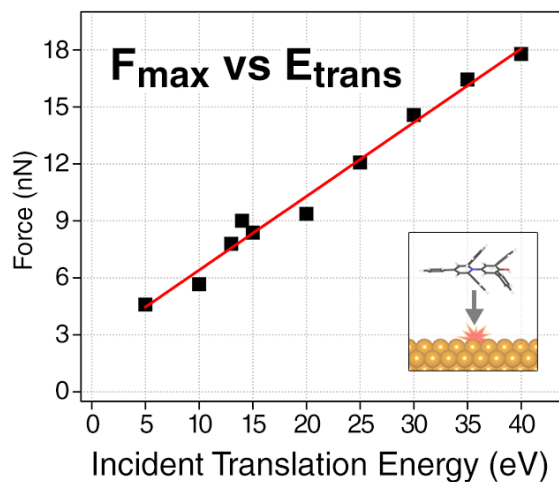
**Supporting Information Fig S3. Ground electronic structure of RD/Cu(100) system.** The charge in the molecule located  $7 \text{ \AA}$  above the surface was computed to be  $+0.6 e$ , indicating a cationic species, while the charge in the Cu-slab was computed to be  $-0.6 e$ . The excess electron in the Cu-slab was computed to mainly localize above the first layer of the surface (green density, isosurface:  $0.0002 e\text{\AA}^{-3}$ ), as shown by the charge difference density ( $\rho_{\text{mol+surf}} - \rho_{\text{mol}} - \rho_{\text{surf}}$ ) in the Cu-slab. Such a configuration is indicative of charge polarization of a conductor by a nearby point charge.



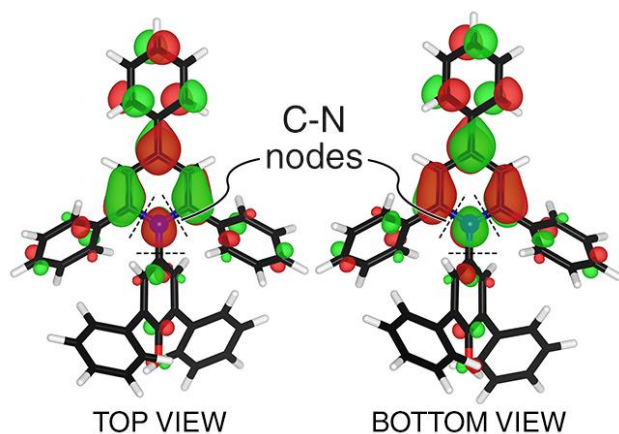
**Supporting Information Fig S4. Fitting of collision model into the experiment and ab-initio results.**

The fit to experimental data used the energy-profile-broadened version of the fitting equation (see Eq (2) in Methods), while the fitting to ab-initio molecular dynamics results used the non-broadened version of the fitting equation (see Eq (1) in Methods). The fit was performed by enforcing a normalization condition whereby the sum of probabilities from three outcome (CRACK, SPLIT, INTACT) must equal to unity at all collision energies.





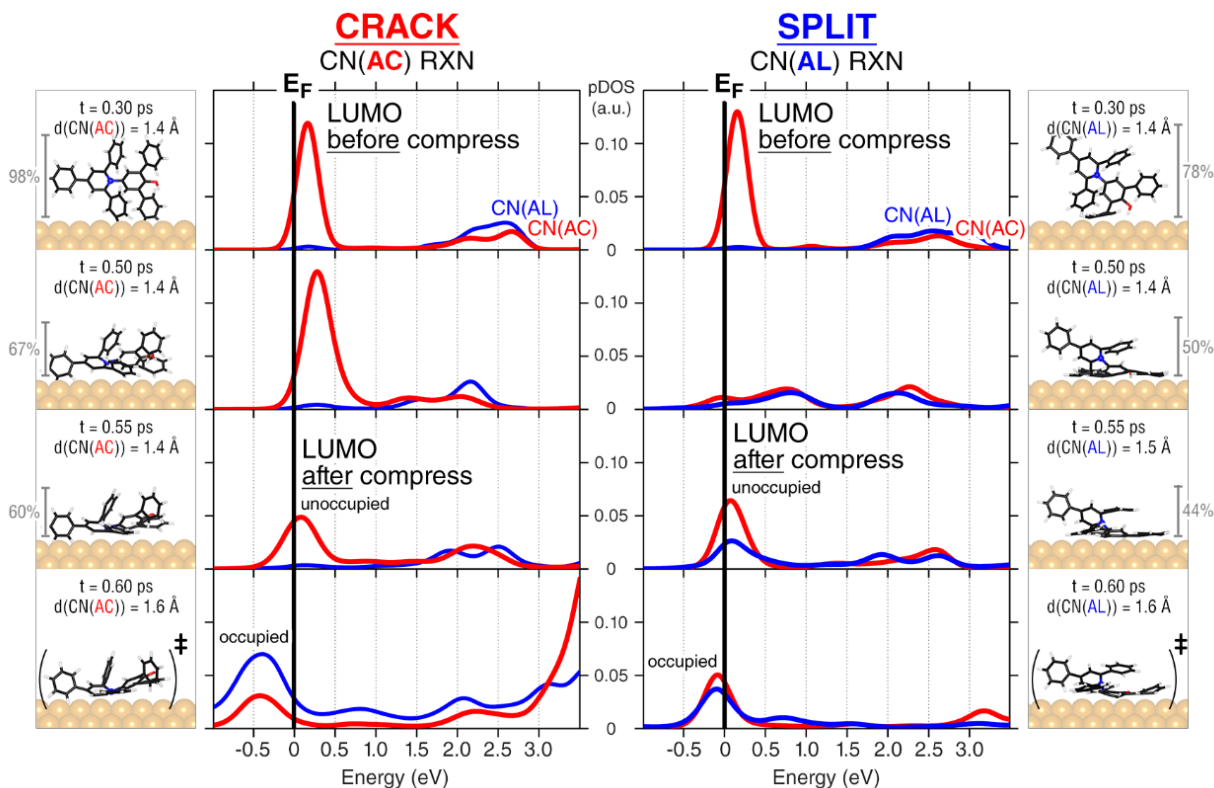
**Supporting Information Fig S5. Dependence of maximum stopping force on collision energy.** The peak force obtained from the MD calculations was found to be linear with respect to the collision energy of the molecule to the surface, as shown by the linear fit (red line). The forces shown here are only for a single orientation of RD with its NO-axis parallel to the surface plane (see inset).



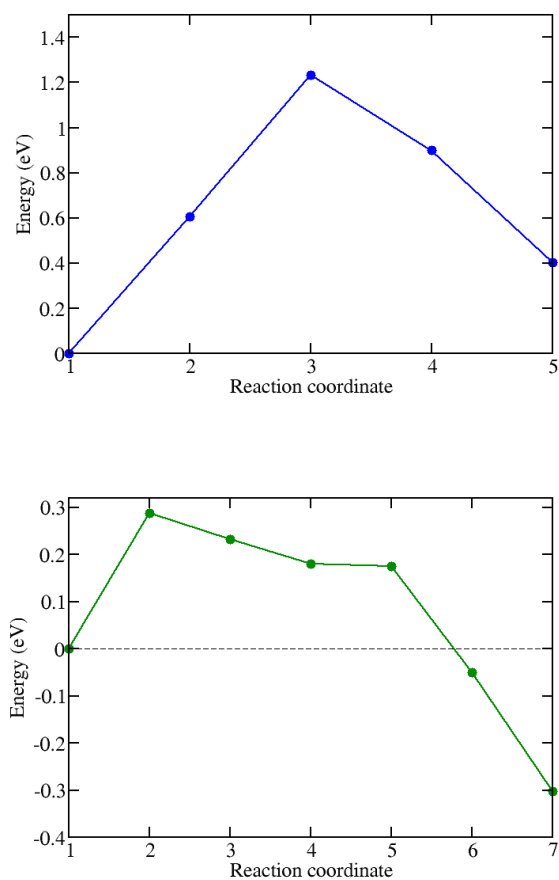
**Supporting Information Fig S6. Computed LUMO for a singly-protonated RD in gas-phase. (A)**

The LUMO was computed to be a  $\pi^*$  antibonding orbital around the C-N bonds (isosurface:  $0.03 \text{ e}\text{\AA}^{-3}$ ).

This is evidenced by the presence of nodal plane (marked by dashed lines) between C- and N-atom in both C-N(AC) and C-N(AL).



**Supporting Information Fig S7. Effect of mechanical compression on RD electronic structure.** The projected density of state (pDOS) shown for the incident RD molecule at different times along the reactive trajectory shown in Fig 4 of the main text. The pDOS shows (i) the LUMO to be mixing differently depending on the compression direction; and (ii) charge flow from the surface to the LUMO during the concurrent dissociation of the C-N bond and formation of C-Cu bond to the surface (i.e. going from  $t = 0.55$  ps to  $0.60$  ps). The red line gives the density between the C-atom and the N-atom in C-N(AC), while the blue line, for C-N(AL).



**Supporting Information Fig S8. Minimum energy pathways and energy barriers for the CRACK and SPLIT.** The upper panel gives the MEP for CRACK, and the lower panel, for SPLIT. Five and seven images (along the reaction coordinate) were used for CRACK and SPLIT, respectively. The barrier for CRACK is found to be 1.23 eV, the one for SPLIT is 0.28 eV.

**Supplementary Video 1. Computed dynamics for CRACK pathway.** The trajectory shows C-N(AC) to be broken upon the molecule impacting the surface. The movie was rendered at 30 fps.

**Supplementary Video 2. Computed dynamics for SPLIT pathway.** The trajectory shows C-N(AL) to be broken upon the molecule impacting the surface. The movie was rendered at 30 fps.